Physical Science International Journal

22(3): 1-12, 2019; Article no.PSIJ.49908
ISSN: 2348-0130

The Vacancy Energy in Metals: Cu, Ag, Ni, Pt, Au, Pd, Ir and Rh

T. H. Akande[1*], F. Matthew-Ojelabi[1], G. S. Agunbiade[1], E. B. Faweya[1] and A. O. Adeboje[2]

[1]Department of Physics, Ekiti State University, P.M.B. 5363, Ado Ekiti, Nigeria.
[2]Department of Physics, Alex Ekwueme Federal University, Ndufu-Alike, Ikwo, Ebonyi State, Nigeria.

Authors' contributions

This work was carried out in collaboration among all authors. All authors read and approved the final manuscript.

Article Information

DOI: 10.9734/PSIJ/2019/v22i330132
Editor(s):
(1) Dr. Mohd Rafatullah, Division of Environmental Technology, School of Industrial Technology, Universiti Sains Malaysia, Malaysia.
(2) Dr. Roberto Oscar Aquilano, School of Exact Science, National University of Rosario (UNR), Rosario, Physics Institute (IFIR)(CONICET-UNR), Argentina.
Reviewers:
(1) Francisco Bulnes, Tecnológico de Estudios Superiores de Chalco, Mexico.
(2) Snehadri Ota, India.
(3) A. Ayeshamariam, Khadir Mohideen College, India.
(4) Adel H. Phillips, Ain-Shams University, Egypt.
Complete Peer review History: http://www.sdiarticle3.com/review-history/49908

Original Research Article

Received 18 April 2019
Accepted 29 June 2019
Published 08 July 2019

ABSTRACT

The predictive calculations of vacancy formation energies in metals: Cu, Ag, Ni, Pt, Au, Pd, Ir and Rh are presented. The energy is given as a function of electron density. Density functional theory underestimates the vacancy formation energy when structural relaxation is included. The unrelaxed mono-vacancy formation, unrelaxed di-vacancy formation, unrelaxed di-vacancy binding and low index surface energies of the fcc transition metals Cu, Ag, Ni, Pt, Au, Pd, Ir and Rh has been calculated using embedded atom method. The values for the vacancy formation energies agree with the experimental value. We also calculate the elastic constants of the metals and the heat of solution for the binary alloys of the selected metals. The average surface energies calculated by including the crystal angle between planes (hkl) and (111) correspond to the experiment for Cu, Ag, Ni, Pt and Pd. The calculated mono-vacancy formation energies are in reasonable agreement with available experimental values for Cu, Ag, Au and Rh. The values are higher for Pt and Ir while smaller values were recorded for Ni and Pd. The unrelaxed di-vacancy binding energy calculated agrees with available experimental values in the case of Cu, Ni, Pt and Au.

**Corresponding author: E-mail: thaiwohassan@gmail.com;*

Keywords: EAM; energy calculations; elastic constants; heats of solutions.

1. INTRODUCTION

Interatomic potential models are numerous but issues on an excellent Interatomic potential model for computer simulation of metallic systems need to be addressed. Although there are so many developed models like effective medium theory (EMT), Glue model, modified embedded atom model (MEAM), model generalized pseudo-potential theory (MGPT) e.t.c, but the embedded-atom method (EAM) is an extensively used technique [1] for the understanding of many-body potential models.

Using the EAM, the energy need to position an impurity atom in a lattice is taken as a function of the electron density. An atomic species at a particular site therefore has an unmatched energy function of the electron density [2]. Through this belief, many authors have originated several potential models. Finnis and Sinclair developed a model which is mathematically analogous to the EAM [3]. The functional form of the energy of the EAM was deduce [4], [5] using density-functional theory. Johnson developed a simple analytic model for fcc (face-centered cubic) metals using nearest neighbor distance [6]. This EAM function is sufficient only for nearest-neighbor interaction and the reliability has been investigated by calculating the vacancy energy in some selected fcc metals. A closet analytic form of embedding function has been procured by chosen exponential charge density of interest [7], and potential parameters for fcc metals was obtained using a third neighbor model. The embedding energy of an atom should take the total form of energy [8] as presented by Banerjea and Smith [9].

There is existence of defect in a crystal lattice at temperatures above absolute zero and the presence of small amount of impurities may enhance vacancy formation in many metals and metal alloys [10]. Thermodynamics has provided the possibility of estimating the defect concentrations of metals at the equilibrium conditions even with good inter atomic potentials. For proper understanding of the defect trapping during solidification in pure metals, molecular dynamics simulations for both aluminum and nickel has been performed and found that vacancies are dominant defects in the product crystals of both metals [11].

It is now clear that everyone has the choice of potentials and embedding energy but the most excellent ones are those that can reproduce the significant parameters of the metals and alloys. In this paper, the employed potential utilized the total form of the embedding function presented by Mayer with two-body potential of Rose et al [12]. This potential function was selected for it is very simple form and easy to be used in computer simulation. The potential parameters of this model are derived through fitting the lattice constant, elastic constants, cohesive energy, and vacancy formation energy by optimization technique. A new 3D metal-vacancy solid-solution for NiAlP has been synthesized by combining selective alkali-etching and phosphorization strategies as a highly-active and earth-abundant pH bifunctional electrocatalyst for efficient water splitting [13]. Vacancy coalescence of metallic oxide/alloy interface can result in the formation of low-density metal and eventually small sized voids [14].

The parameters of the EAM have been used to calculate properties including bulk modulus, monovacancy forming energy, divacancy forming energy, divacancy binding energy, the surface energy of the low index crystal, and the elastic constants. Information concerning the ground state properties of these metals is significant in mandate to know the kind of materials that can be formed from such metals. An embedded atom method potential for Ni-Al alloys has been procured [15]. Their declaration of the embedded function was devised in analogy with the density function theory. Consistent empirical embedded-atom potential that contains a long range force for fcc metals and alloys has been developed to estimate the elastic constants and the heats of solution of some choice fcc metals [16]. The total energy of EAM is given as

$$E_{tot} = \sum_i F_i(\rho_i) + \frac{1}{2}\sum_{i,j} \phi_{ij}(r_{ij}) \quad (1)$$

Where

$$\rho_i = \sum_{j \neq i} f_{ij}(r_{ij}) \quad (2)$$

The parameter $F_i(\rho_i)$ is the energy to embed an atom into the environment of the remaining atoms, ϕ_{ij} is an electrostatic two-body interaction between atoms i and j and $f_{ij}(r_{ij})$ is the local electron density, ρ is the host electron density. So far, from equation (1) the following functions $F(\rho)$, $\rho(r)$ and $\phi(r)$ are very important.

2. THEORY

In the Analytic Embedded Atom Method, the electron density is given by:

$$f(r) = f_e exp\left[-\beta\left(\frac{r}{r_o} - 1\right)\right] \quad (3)$$

The embedding potential between atom i and atom j is given by:

$$\phi^{ij}(r) = \phi_e exp\left[-\gamma\left(\frac{r}{r_o} - 1\right)\right] \quad (4)$$

The embedding function is determined using equation (5):

$$F(\rho) = -E_c\left[1 - \frac{\alpha}{\beta} ln\left(\frac{\rho}{\rho_o}\right)\right]\left[\frac{\rho}{\rho_o}\right]^{\frac{\alpha}{\beta}} - \Phi_e\left[\frac{\rho}{\rho_o}\right]^{\frac{\gamma}{\beta}} \quad (5)$$

where $\rho_o = 12f_e$ and $\Phi_e = 6\phi_e$

To determine the two adjustable parameters f_e and ϕ_e for each metal, equation (6) was used. $f_e = \frac{SE_c}{\Omega_e}$ and

$$\phi_e = \frac{E_c}{6} \quad (6)$$

where S is an arbitrary scaling constant. The parameters α, β and γ can easily be determined from equations (7 – 9).

$$\alpha = 3\left(\frac{\Omega_e B}{E_c}\right)^{\frac{1}{2}} \quad (7)$$

$$\beta = \left(\frac{15E_c\Omega_e G}{E_v(E_v+E_c)}\right)^{\frac{1}{2}} \quad (8)$$

$$\gamma = \left(\frac{15\Omega_e G(E_c+E_v)}{E_c E_v}\right)^{\frac{1}{2}} \quad (9)$$

The elastic constants C_{11}, C_{12} and C_{44}, were calculated using equations (10), (11) and (12):

$$C_{11} = \frac{a_o^2}{2\Omega_e}\left[\left\{\varphi_e^{''}(r) - \frac{1}{r_o}\varphi_e^{'}(r)\right\} + 2F^{'}(\rho_e)\left\{f_e^{''}(r) - \frac{1}{r_o}f_e^{'}(r)\right\}\right] \quad (10)$$

$$C_{12} = \frac{a_o^2}{4\Omega_e}\left[\left\{\varphi_e^{''}(r) - \frac{1}{r_o}\varphi_e^{'}(r)\right\} + 2F^{'}(\rho_e)\left\{f_e^{''}(r) - \frac{1}{r_o}f_e^{'}(r)\right\}\right] + \frac{8a_o^2}{\Omega_e}\left(f_e^{'}(r)\right)^2 F^{''}(\rho_e) \quad (11)$$

$$C_{44} = \frac{a_o^2}{4\Omega_e}\left[\left\{\varphi_e^{''}(r) - \frac{1}{r_o}\varphi_e^{'}(r)\right\} + 2F^{'}(\rho_e)\left\{f_e^{''}(r) - \frac{1}{r_o}f_e^{'}(r)\right\}\right] \quad (12)$$

The bulk modulus B and the shear modulus G, in equations (7 – 9) is determined from equations (13) and (14) respectively.

$$B = \frac{1}{3}(C_{11} + 2C_{12}) \quad (13)$$

$$G = \frac{1}{5}(C_{11} - C_{12} + 3C_{44}) \quad (14)$$

2.1 Energy Calculations

Vacancy migration which most often leads to vacancy forming is the controlling movement behind atomic carriage in most elemental crystals, and is of underlying consequence in procedure similar to solid phase transformations and fault migration. Vacancy formation implies the removal of an atom from the interior of a crystal. At thermal equilibrium as the vibration increases with increasing energy, the orientation of the atoms within the crystal changes. At lower thermal energy, the atoms are relaxed to a state of quasi thermal equilibrium.

The unrelaxed mono-vacancy forming energy is calculated using equations (15) and (16)

$$E_{1v}^{uf} = -12F(\rho_e) + 12F\left(\frac{11}{12}\rho_e\right) - 6\phi_e \quad (15)$$

$$E_{1v}^{uf} = -12E_n + 12E_{n-1} \quad (16)$$

where E_n is the total energy of the system having no vacancy.

The unrelaxed di-vacancy formation energy can be computed using equation (17)

$$E_{2v}^{uF} = -18E_n + 14E_{n-1} + 4E_{n-2} \quad (17)$$

The unrelaxed di-vacancy binding energy is calculated using:

$$E_{2v}^{uB} = 2E_{1v}^{uf} - E_{2v}^{uf} = -6E_n + 10E_{n-1} - 4E_{n-2} \quad (18)$$

The low index surface energy can be computed with equations (19) to (20):

The number of bonds broken on (111) surface $= (3\ bonds/atom)\mathrm{x}\ (1atom/unit\ cell)$

Therefore number of bonds broken on (111) surface = $3/(\frac{\sqrt{3}}{4}a_o^2)$

$$E_{surf} = E_{12-3} = E_9\ ;\ E_{bulk} = E_n = E_{12}$$

$$\therefore \Gamma_{111}^{U} = N_s/A(E_9 - E_{12})$$

where N_s is the number of atom on the surface.

$$\therefore \Gamma_{111}^{U} = \frac{4}{a_o^2\sqrt{3}}(E_9 - E_{12}) \quad (19)$$

Similarly for Γ_{100}^{U} and Γ_{110}^{U} we have

$$\Gamma_{100}^{U} = \frac{2}{a_o^2}(E_8 - E_{12}) \quad (20)$$

$$\Gamma_{110}^{U} = \frac{\sqrt{2}}{a_o^2}(E_7 + E_{11} - 2E_{12}) \quad (21)$$

The crystal angle between planes (*hkl*) and (111) is calculated using

$$cos\theta_{(hlk)} = \frac{(h+l+k)}{\sqrt{3(h^2+k^2+l^2)}} \quad (22)$$

2.2 Alloy Potentials and Heats of Solutions

In computing the alloys pair potentials, the mixing rule (25) in equation (23) was used

$$\phi^{ab}(r) = \frac{1}{2}\left[\frac{f^a(r)}{f^b(r)}\phi^{aa}(r) + \frac{f^b(r)}{f^a(r)}\phi^{bb}(r)\right] \quad (23)$$

and the heats of solution for *b*- type atom as an impurity and *a* -type atom as the host is computed by the summation of equations (24 – 29).

Remove host : $\Delta H_1 = -F^a(\rho_e^a) - \sum \phi^{aa}(r_e^a)$ (24)

Add impurity : $\Delta H_2 = +F^a(\rho_e^a) + \sum \phi^{ab}(r_e^a)$ (25)

Adjust neighbours: $\Delta H_3 = -\sum F^a(\rho_e^a) + \sum F^a(X)$ (26)

where

$$X = \rho_e^a + \Delta\rho \quad (27)$$

and

$$\Delta\rho = -f^a(r_e^a) + f^b(r_e^a) \tag{28}$$

Adjust cohesive energy:

$$\Delta H_4 = -E_c^a + E_c^b \tag{29}$$

Hence,

$$\Delta H = \Delta H_1 + \Delta H_2 + \Delta H_3 + \Delta H_4 \tag{30}$$

It is essential to include lattice relaxations in many calculations involving energies [17]. The relaxation energy is given as:

$$\Delta H_r = -\left[1.167\left(\frac{\Omega_{ea}}{\Omega_{eb}} - 1\right)\right]^2 \tag{31}$$

Here, ρ_e^a is the equilibrium electron density of *a*–type atoms,

Ω_{ea} is the atomic volume of *a* - type atoms and

Ω_{eb} is the atomic volume of b - type atoms.

Table 1. Experimental data used in fitting procedure are: equilibrium lattice constants (a_o), cohesive energy E_c, vacancy formation energy E_{1v}^{uf} and the elastic constants: (C_{11}, C_{12}, C_{44} in $ergcm^{-3}$(column 5 - 7)) and $eV/\text{Å}^3$ (column 8 – 10). The elastic constants: C_{11}, C_{12}, C_{44} in the last three column was converted from $ergcm^{-3}$ to $eV/\text{Å}^3$

S/N	Atom	a_o(Å)	E_c (eV)	E_{1v}^{uf} (eV)	C_{11}	C_{12}	C_{44}	C_{11}	C_{12}	C_{44}
1	Cu	3.615[a]	3.54[c]	1.30[h]	1.670[a]	1.240[a]	0.760[a]	1.04	0.77	0.47
2	Ag	4.090[a]	2.85[c]	1.10[h]	1.240[b]	0.934[b]	0.461[b]	0.77	0.58	0.29
3	Ni	3.520[a]	4.45[c]	1.70[i]	2.465[b]	1.473[b]	1.247[b]	1.54	0.92	0.78
4	Pt	3.920[a]	5.77[c]	1.60[i]	3.470[b]	2.510[b]	0.765[b]	2.17	1.57	0.48
5	Au	4.080[c]	3.93[c]	0.90[h]	1.860[b]	1.570[b]	0.420[b]	1.16	0.98	0.26
6	Pd	3.890[c]	3.91[c]	1.54[i]	2.341[b]	1.760[b]	0.712[b]	1.46	1.10	0.44
7	Ir	3.840[c]	6.94[c]	1.80[d]	5.990[b]	2.560[b]	2.690[b]	3.74	1.60	1.68
8	Rh	3.800[c]	5.75[c]	1.71[g]	4.220[b]	1.920[b]	1.940[b]	2.63	1.20	1.21

Refs: [a][17] ; [b][18]; [c][19]; [d][20]; [e][21]; [f][22]; [g][23]; [h][24]; [i][25]; [j][26]

3. RESULTS AND DISCUSSION

The calculated surface energies for the low index crystal faces are compared to the experimental polycrystalline average values (eV/cm^2). The values indicated by an asterisk was extrapolated from the melt temperature down to 0K [32].

In Fig. 1, the electron density $f(r)$ displays the common characteristics for the selected metals.

Fig. 2 shows the least (minimum) free energy curves for the electron which gives the equilibrium interatomic distance. The width of the curves increases as the values of *r* increases, therefore the position of the principal minimum is displaced to larger values of *r*. The pair-potential tends to group Cu, Ag, Ni, Pt, Au and Pd, also Ir and Rh.

In Fig. 3, there are systematic trends in the embedding energies. The curvature of the embedding function accounts for the "many-body" aspect of the model with the least embedding energy occurring for Ir.

Fig. 4 shows that the embedding function goes through the appropriate range of electron densities and the characteristics curves tends to group: Cu, Pd with Au and also Pt with Rh.

Table 2. Calculated input parameters Ω_e, B, G and model parameters f_e, φ_e, α, β and γ

S/N	Metal	$\Omega(\text{Å}^3)$	B(eV/Å^3)	G(eV/Å^3)	$f_e(eV)$	$\varphi_e(eV)$	α	β	γ
1	Cu	11.81	0.86	0.34	0.30	0.59	5.09	5.81	7.94
2	Ag	17.10	0.65	0.21	0.17	0.47	5.91	5.96	8.26
3	Ni	10.90	1.13	0.59	0.41	0.74	4.98	6.41	8.86
4	Pt	15.06	1.77	0.41	0.38	0.96	6.44	6.70	8.56
5	Au	16.98	1.04	0.19	0.23	0.66	6.36	6.67	8.20
6	Pd	14.72	1.22	0.34	0.27	0.65	6.43	5.90	8.23
7	Ir	14.16	2.31	1.44	0.49	1.16	6.51	10.98	14.09
8	Rh	13.72	1.68	1.01	0.42	0.96	6.00	12.05	14.54

Table 3. Calculated formation $E_{2v}^{uF}(eV)$, binding $E_{2v}^{uB}(eV)$, and low index surface $\Gamma_{(hlk)}^{U}(\frac{ergs}{cm^2})$ energies. The present work is listed first (values with asterisk include $cos\theta_{(hlk)}$). The experimental values are listed second, and the results of other authors are listed last

S/N	Atom	$E_{2v}^{uF}(eV)$	$E_{2v}^{uB}(eV)$	$E_{1v}^{uf}(eV)$	$\Gamma_{111}^{U}\mathbf{x10^3}$	$\Gamma_{100}^{U}\mathbf{x10^3}$	$\Gamma_{110}^{U}\mathbf{x10^3}$	$\Gamma_{ave}^{U}\mathbf{x10^3}$
1	Cu	2.41	0.19 0.13±0.04[l] , 0.3[m] 0.27[a]	1.31 1.3[h] 1.28[a]	1.02, 1.02*	1.23, 2.14*	1.34, 1.64*	1.20, 1.60 1.77[q] 1.28[a], 1.57[q]
2	Ag	2.13	0.15 0.38[n] 0.22[a]	1.14 1.10[h]	0.70, 0.70*	0.86, 1.49*	0.94, 1.15*	0.83, 1.11 1.32[q] 0.70[a], 1.19[q]
3	Ni	3.15 2.92– 3.10[a*]	0.27 0.33[p], 0.28[l*] 0.44[a]	1.71 1.80[d]	1.32, 1.32*	1.56, 2.71*	1.69, 2.06*	1.52, 2.03 2.24[q]
4	Pt	3.29	0.19 0.1 – 0.2[h] 0.45[a]	1.74 1.60[i]	1.24, 1.24*	1.56, 2.70*	1.72, 2.10*	1.51, 2.02 2.50** 1.61[a], 1.99[q]
5	Au	1.93	0.09 0.1±0.03[r],0.3[t] 0.22[a]	1.01 0.90[h]	0.70, 0.70*	0.89, 1.54*	0.99, 1.21*	0.88, 1.15 1.54[q] 0.90[a], 1.03[q]
6	Pd	3.10	0.20 0.34[a]	1.65 1.70[i]	1.15, 1.15*	1.41, 2.45*	1.54, 1.89*	1.37, 1.82 2.00** 1.36[a], 1.57[q]
7	Ir	3.64	0.32	1.98 1.80[d]	1.25, 1.25*	1.47, 2.54*	1.58, 1.93*	1.43, 1.91 3.00** 2.84[a]
8	Rh	3.14	0.28	1.71 1.71[g]	0.78, 0.78*	0.91, 1.58*	0.98, 1.20*	1.28, 1.72 2.60**

Refs: [a][17] ; [d][20]; [e][21]; [g][39]; [h][24][l];[25] ; [j][26] ; [l][27]; [l][28] ; [m][29]; [n][30] ; [p][31] ; [q][32] [r][33]; [t][34] ; [u][35]; [a*][36]*

Table 4. Calculated and experimental properties of pure metals. The first lines present the experimental values of elastic constants in $eV/\text{Å}^3$ (column 3 – 5) and Bulk modulus in $eV/\text{Å}^3$ (column 6). The second lines present the predicted values using common cut-off radius $1.11r_e \geq r_c \leq 1.25r_e$

S/N	Metal	C_{11}	C_{12}	C_{44}	B
1	Cu	1.04[a]	0.77[a]	0.47[a]	0.86[g]
		1.03	0.57	0.53	0.72
2	Ag	0.77[b]	0.58[b]	0.29[b]	0.60[g]
		0.77	0.43	0.40	0.54
3	Ni	1.54[b]	0.92[b]	0.78[b]	1.16[g]
		1.53	0.84	0.79	1.07
4	Pt	2.17[b]	1.57[b]	0.48[b]	1.77[g]
		1.87	1.02	0.96	1.30
5	Au	1.16[b]	0.98[b]	0.26[b]	1.08[g]
		1.18	0.65	0.61	0.83
6	Pd	1.46[b]	1.10[b]	0.44[b]	1.21[g]
		1.66	0.97	0.88	1.20
7	Ir	3.74[b]	1.60[b]	1.68[b]	2.22[b]
		3.72	1.97	1.90	2.55[*]
8	Rh	2.63[b]	1.20[b]	1.21[b]	1.68
		2.53	1.33	1.28	1.78

Refs: [a][17]; [b][18] ; [d][20]) ; [f][22] ; [g][23] ; [*]Computed using equation (8)

Table 5. Heats of solution for the likely binary alloys of the chosen fcc metals. The results of the unrelaxed calculations are listed first, the values with relaxation second, the experimental values (Ref. v and w) where valid, and the adapted values from other author (Ref. q and y) are listed last

Impurity	Host							
	Cu	Ag	Ni	Pt	Au	Pd	Ir	Rh
Cu		0.40	0.11	-0.19	0.05	0.10	-0.29	-0.17
		0.27	0.10	-0.26	-0.08	0.05	-0.33	-0.20
		0.25[v]	0.11[v]	-0.30[v]	-0.13[v]	-0.39[v]	-0.64[q]	-0.72[q]
Ag	0.79		1.88	0.65	-0.06	0.32	1.37	1.12
	0.52		1.44	0.63	-0.06	0.28	1.31	1.02
	0.39[v]				-0.16[v]	-0.11[v]	0.78[q]	
Ni	0.08	0.75		-0.12	0.33	0.22	-0.34	-0.14
	0.07	0.57		-0.23	0.19	0.21	-0.41	-0.20
	0.03[v]			-0.33[v]	0.22[v]	-0.09[v]	-0.25[q]	-0.35[q]
Pt	-0.30	0.66	-0.23		0.46	-0.03	0.17	0.02
	-0.40	0.64	-0.43		0.46	-0.03	0.16	0.01
	-0.53[v]		-0.28[v]					
Au	-0.01	-0.03	0.84	0.58		-0.03	1.47	0.91
	-0.27	-0.03	0.42	0.56		-0.06	1.42	0.84
	-0.19[v]	-0.19[v]	0.28[v]			-0.20[v]	0.57[q]	0.37[q]
Pd	0.15	0.30	0.69	-0.01	0.01		0.43	0.26
	0.06	0.28	0.53	-0.01	-0.01		0.43	0.25
	-0.44[v]	-0.29[v]	0.06[v]		-0.36[v]			
Ir	-0.94	0.66	-1.29	0.07	0.51	-0.06	-	0.004
	-0.99	0.62	-1.41	0.06	0.47	-0.06		0.006
	-0.73[q]	0.55[q]	-0.68[q]		0.38[q]	-0.28[q]		
Rh	-0.44	0.52	-0.47	-0.01	0.32	0.03	-0.04	-
	-0.48	0.47	-0.56	-0.00	0.27	0.03	-0.04	
	-0.74[q]	0.35[q]	-0.55[q]		0.24[x]	-0.35[q]		

Refs: [q][32]; [w][37] ; [v][38] ; [y][16])

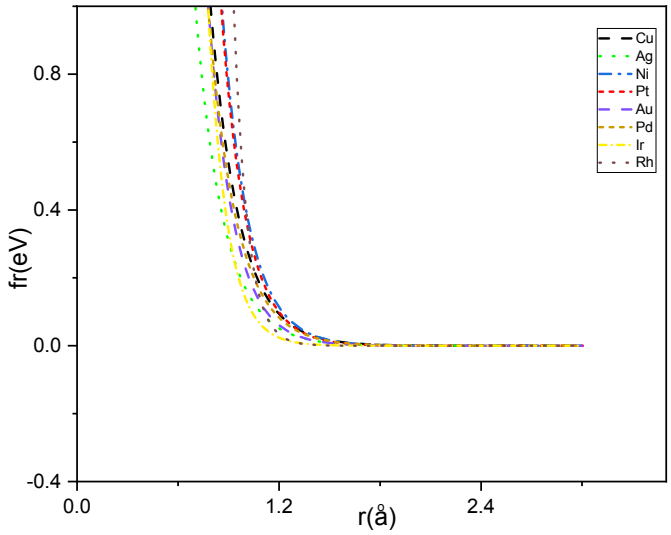

Fig. 1. Characteristics of the electron density function for the selected metals

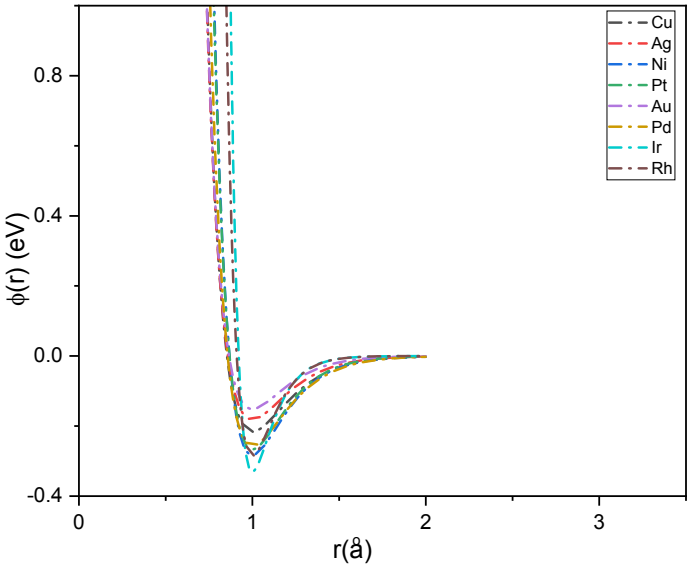

Fig. 2. Characteristics of the pair-potential function for the selected metals

Fig. 5 presents the unrelaxed surface energies for the selected metals while Figs. 6 and 7 give the plots of the unrelaxed mono-vacancy formation and di-vacancy binding energies respectively.

The properties calculated in this work will help in finding new metals/compounds for substitution in alloying processes. The ground state properties such as, surface energies, vacancy formation energies and heats of solutions has been calculated. The sensitivity of the heats of solutions on the embedding function and the potential produces good results in comparison with the available experimental values.

Finding new metals/compounds for substitution in alloying processes is an issue that needs to be addressed by the material scientist especially in this state of scarcity in the case of palladium. The calculated mono-vacancy formation energies are in reasonable agreement with available experimental values for Cu, Ag, Au and Rh as shown in Fig. 6. The values are higher for Pt and

Ir while smaller values were recorded for Ni and Pd. The unrelaxed di-vacancy binding energy calculated agree with available experimental values closer than the results of ref. [17] in the case of Cu, Ni, Pt and Au (See Fig. 7).

The unrelaxed surface energy for the three fcc low-index planes was estimated by dividing the total energy increase in separating bulk material on a crystallographic plane by the total new surface area created. In all the cases, the trends $E_{(111)} < E_{(100)} < E_{(110)}$ was observed and also by including crystal angle between planes, we have $E_{(111)} < E_{(110)} < E_{(100)}$. The lowest surface energy corresponds to the closed-packed (111) plane as observed in Table 3. Therefore closed packed surfaces looks most stable for fcc metals. The calculated average surface energies are closer to the experimental values than those obtained by the MEAM [32].

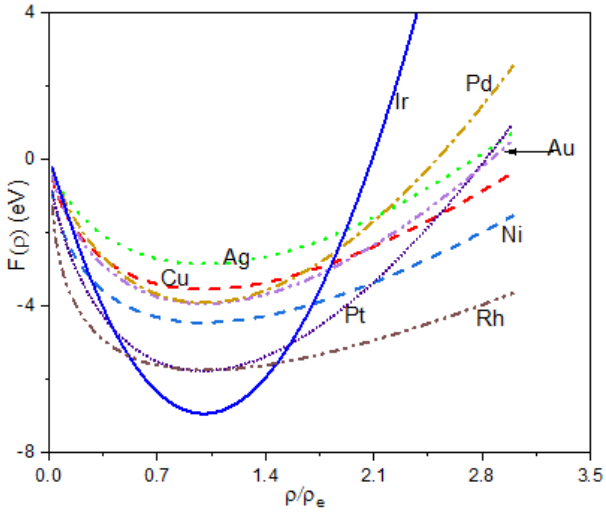

Fig. 3. Characteristics of the embedding energy function for the selected metals

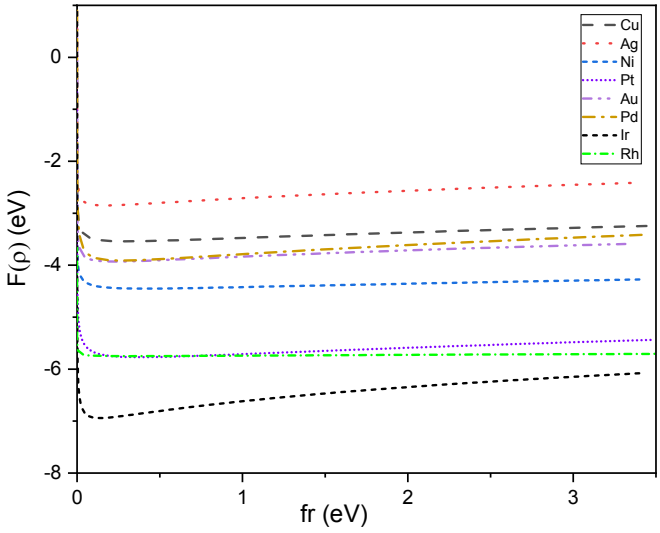

Fig. 4. Characteristics of the embedding energy function with electron density for the selected metals

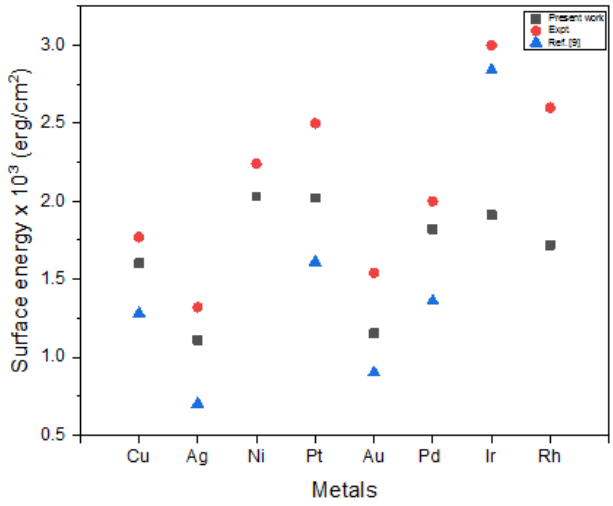

Fig. 5. Plot of unrelaxed surface energies for the selected metals

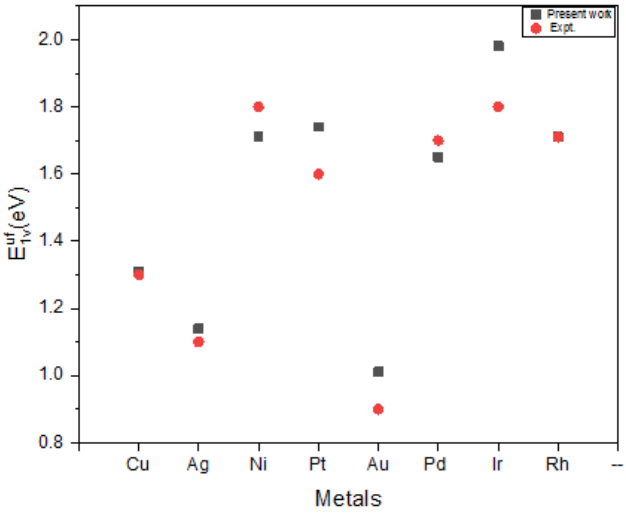

Fig. 6. Plot of unrelaxed mono-vacancy formation energies for the selected metals

The average surface energies predicted low average values compared to the available experimental values but when the crystal angle was included, moderate average values were obtained and they are in good agreement with the available experimental values for Cu, Ag, Ni, Pt and Pd. The results for Cu, Pt, Au and Pd are closer to the experimental values than that of ref. [17] (See Fig. 5) and [32] (See Table 3).

4. SUMMARY

The calculated ground state properties for the pure metals include surface energies, mono-vacancy formation energies, di-vacancy formation energies, di-vacancy binding energies, elastic constants and their heats of solutions. The agreement between the experiment and the calculated values is quite good for the metals and their alloys. From the heats of solutions calculated (Table 5), the positive heats of solution recorded are higher than the negative heats of solutions. The most negative heats of solution occur for the relaxation values and most positive occurs for the unrelaxed values. The pair potential function of the alloy mixing '$\varphi(r)^{ab}$' between two different atoms *a* and *b* gives reasonable values of heats of solutions in the case of Cu, Ag, Au, Ni and Pt.

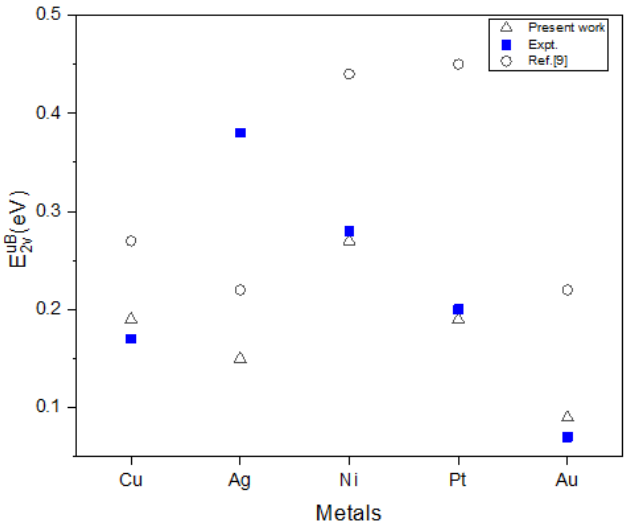

Fig. 7. Plot of unrelaxed di-vacancy binding energies for some of the selected metals

5. CONCLUSION

The EAM model was used to compute some ground state properties of the selected fcc transition metals and their binary alloys. The di-vacancy binding energies calculated also agree with the available experimental values. The surface energies predicted by the model was low in comparison to experiments but when the crystal angle was included, the model predicted low index surface energies that agree reasonably with the experiment in better comparison with the values from ref. [17] and [32]. The model is well-suited for studies of defects energies in metals and their alloys. The surface energies calculated by including the crystal angle between planes corresponds to the experiment for Cu, Ag, Ni, Pt and Pd. For surface energy minimization, it is good that the (111) texture should be favoured in an fcc film. The embedding function $F(\rho)$ with the angle between planes (*hkl*) and (111) can be used to estimate the relative values of surface energy for surfaces in different orientations.

COMPETING INTERESTS

Authors have declared that no competing interests exist.

REFERENCES

1. Daw MS, Bisson CL, Wilson WD. Solid Commun. 1983;46.
2. Puska J, Nieminen RM, Manninen M. Phys. Rev. B. 1981;24:3037.
3. Finnis MW, Sinclair JE. Philos. Mag. A. 1984;50:45.
4. Manninen M. Phys. Rev. B. 1986;34:8486.
5. Jacobson KW, Nárskov JK, Puska J. Phys. Rev. B. 1987;35:7423.
6. Johnson RA. Phys. Rev. B. 1988;37:3924.
7. Mei J, Devenport JW, Fernando G.W. Phys. Rev. B. 1990;43:4653.
8. Cai J, Ye YY. Phys. Rev. B. 1996;54:8398.
9. Banerjea A, Smith JR. Phys. Rev. B. 1988; 37:6632.
10. Laura Bukonte. Modelling of defect formation and evolutionin metals and silicon. Division of Materials Physics, University of Helsinki-Helsinki, Finland. 2017;1-66.
[ISBN: 978-951-51-2768-6]
11. Zhang HY, Lu F, Yang Y, Sun DY. Scientific Reports. 2017;7(10241):1-8.
12. Rose JH, Smith JR, Guinea F, Ferrante J. Phys. Rev. B. 1984;29:2963.
13. Cheng Weiren, Zhang Hui, Zhao Xu, Su Hui, Tang Funmin, Tian Jie, Lui Quinghua Journals of Materials Chemistry A. 2018; 20:1- 19.
14. Richard P. Oleksak, Monica Kapoor, Daniel E. Perea, Gordon R. Holcomb, Ömer N. Doğan. Npj Materials Degradation. 2018;25:1-8.
15. Zhang RF, Liu BX. Proposed model for calculating the standard formation enthalpy of binary transition-metal systems. *Appl.* Phys. Lett. 2002;81:1219–1221.
16. Iyad AH, Young P. J. Mater. Sci. Technol. 2009;25:6.

17. Foiles SM, Baskes MI, Daw MS. Phys. Rev. B. 1986;33:7983.
18. Simmons G, Wang H. Single crystal elastic constants and calculated aggregate properties: A handbook (MIT Press, Cambridge); 1971.
19. Kittel C. Introduction to solid state Physics. 7th edition. John Willey and Sons. Inc., New York, Chicester, Brisbarne, Toronto, Singapore. 1996;28–98.
20. Landolt-Börnstein. New Series, Vols. III-11 and III-18 Berlin: Springer-Verlag; 1991.
21. Ziesche P, Perdew JP, Fiolhais C. Spherical voids in the stabilized Jellium model: Rigouruos theorems and pad; Representation of the Void-Formation Energy. Phy. Rev. B. 1994;49:7916.
22. Sisoda P, Verma MP. Shear moduli of polycrystalline cubic elements. J. Phys. Chem. Solids. 1989;50:223–224.
23. De Boer FR, Boom R, Mattens WCM, Miedema AR, Niessen AK. Cohesion in Metals, Amsterdam: North Holland. 1988;1.
24. Ballufi RW. J Nucl. Matter. 1978;69(70): 240.
25. Johnson RA. Phys. Rev. B. 1989;39(17): 12554–12559.
26. Ghorai A. Physica Status Solidi B. 1991; 167:551.
27. Seeger A, Gerold V, Chik KP, Ruhle M. Phys. Letters. Netherlands. 1963;6 :107.
28. Seeger A, Schumacher D. Mater. Sci. Eng. 1967;2:31.
29. Fluss MJ, Smedskjaer LC, Siegel RW, Longini DG, Chason MK. J. Phys. F. 1980;10:1763.
30. Kraftmakher YA, Strelkov PG. In vacancies and interstitials in metals, edited by Seeger A, Schumacher D, Schilling W, Diehl J. (North-Holl and), Amsterdam. 1970;59.
31. Mehrer H, Kbonmuller H, Seeger H. Phys. Stat. Sol. 1965;10:725.
32. Baskes MI. Phys. Rev B. 1992;46:2727.
33. Bauerle JE, Koehler JS. 1957;107:1493.
34. Meshii M, Mori T, Kauffman JW. Phys. Rev. 1962;185:1239.
35. Ehrhart P, Jung P, Schultz H, Ullmaier H. Atomic defects in metals. Springer verlag. Edited by Ullmaier H. Landolt-Börnstein. New Series. Group III/25, Berlin; 1991.
36. Nanao S, Kuribayashi K, Tanigawa S, Doyama M. J. Phys. F: Met. Phys. 1977; 7:1403.
37. Miedema AR, de`Chatel PF, de Boer FR. Physica B. 1980;100:1.
38. Hultgren R, Desai PD, Hawkins DT, Gleiser M, Kelley KK. Selected values of the thermodynamic properties of binary alloys (American Society for Metals, Metals Park, OH); 1973.
39. Ledbetter H, Kim S. Monocrystal elastic constants and derived properties of the cubic and the hexagonal elements, in: Handbook of elastic properties of solids, liquids and gases, Academic Press. 2001;2.

Peer-review history:
The peer review history for this paper can be accessed here:
http://www.sdiarticle3.com/review-history/49908